

Detailed feasibility study of a gamma ray detector system for nanosatellites using GEANT4 simulations

Galgócz Gábor, Fizikus MSc szak, 3. évfolyam*

Eötvös Loránd Tudományegyetem, Természettudományi Kar

WIGNER Fizikai Kutatóközpont - MTA



Témavezető:

Norbert Werner (ELTE)

2018

Contents

1	Introduction	1
1.1	Gamma-ray bursts	3
1.2	Open questions on gamma-ray bursts	5
1.3	Search for the electromagnetic counterparts of gravitational wave events	6
1.4	Particle detectors in space	7
1.5	Current missions observing gamma-ray bursts	7
1.6	The CAMELOT satellite	9
1.7	The detection of GRBs	11
1.8	The Geant4 platform	12
1.9	The experimental setup	13
1.10	The readout of the detector	16
1.11	1 channel setup	18
1.12	2 channel read out setup	19
1.13	The satellite	20
2	Results of the simulation	21
2.1	Comparison of the results of the simulation with experiments	21
2.1.1	X-ray fluorescence	22
2.1.2	Calibration of the position dependence	23
2.1.3	Calibration of photon yield	24
2.2	Simulation of the signal induced by GRBs in the satellite	25
2.3	Simulation of the cosmic background in space	26
2.3.1	Proton background	26
2.4	Electron background	26
3	Conclusion	28
4	Acknowledgment	30
References		31

Introduction

The main aim of this thesis is to simulate the detection of γ -rays from GRBs with the Constellation Gamma (Camelot) CubeSats (miniaturized satellites). The Geant4 simulation described in this paper also predicts the background signal originating from solar and cosmic protons and electrons.

First the parameters of the simulation had to be fine tuned to reproduce the measured spectra in the laboratory. The simulation of the number of optical photons being detected was sufficient to predict the signal as the electronic amplification is linear.

The build up of the satellite is quite complex, consisting of 9 modules, each with a specific material composition. Therefore the CAD model of the satellite was imported into Geant4 in order to understand how the satellite itself would affect the measurements. The "calibrated" scintillator afterwards was placed on the side of the satellite.

Three cases were investigated. First, the model of the detector and the satellite was radiated with a parallel gamma beam that had the same parameters as GRB 9900123, the reference GRB chosen. The position of the source was rotated spherically around the satellite. In this way the absorption of γ s in the material of the satellite was investigated.

Secondly the cosmic background induced by the protons and electrons was simulated. The energy spectrum of electrons and protons was obtained from the SPENVIS information system. The satellite was radiated with these given energy distributions and fluxes.

We are designing a fleet of nanosatellites to perform accurate position determinations of short-duration gamma-ray bursts by measuring arrival time differences. To achieve sufficient photon statistics to measure the arrival times precisely under the severe limitations of size, mass, and power consumption, we propose the use of a large-area CsI scintillator that has high light output and the use of a small-sized multipixel photon counter (MPPC) that has low power consumption. We plan to use one of the latest-model MPPCs provided by Hamamatsu Photonics, which has an active area of 6 6 mm². We have compared the performance of two scintillators of different sizes (150 75 5 mm³ and 100 75 5 mm³); the bigger one is the maximum size that can be mounted on a three-unit satellite, according to CubeSat standards. We have found that the two scintillators have similar light yields and each has an energy threshold of \sim 10 keV at 25°C. We have also examined the position dependence of the light yield by using radiation from ²⁴¹Am (59.5 keV) source, and have confirmed that uniformity was improved by using two MPPCs for signal

readout.

Gamma-ray bursts

Gamma-ray bursts (GRBs) [1, 2, 3, 4] are one of the most investigated and yet less understood astrophysical objects. They have been studied for more than forty years as one of the most extreme explosive events in the Universe. Their origin is still not yet fully understood. GRBs were discovered in years 1967–73 by military satellites. The scientific community only got to know their existence in the early seventies [5]. A GRB event is brighter than any other object in the sky during their appearance that can last from millisecond to minutes. Every day a new GRB is observed by the satellites investigating them. The main part of the energy spectrum of these events is from the keV to the MeV ranges.

After a decade of investigation it was found that these events can be categorized into two groups by their length [6, 7, 8]. The first group is called long GRBs with softer spectrum and with prompt γ -ray emission of ≥ 2 s. These GRBs were linked to the gravitational collapses of massive stars. These objects are associated with type Ic core-collapse supernovae. The second group of GRBs are called short GRBs as their prompt γ -ray emission lasts ≤ 2 s. These objects also possess a harder spectrum. They were linked to the merge of two very compact objects, such as neutron star - neutron star (NS-NS) and neutron star - black hole (NS-BH) mergers [9].

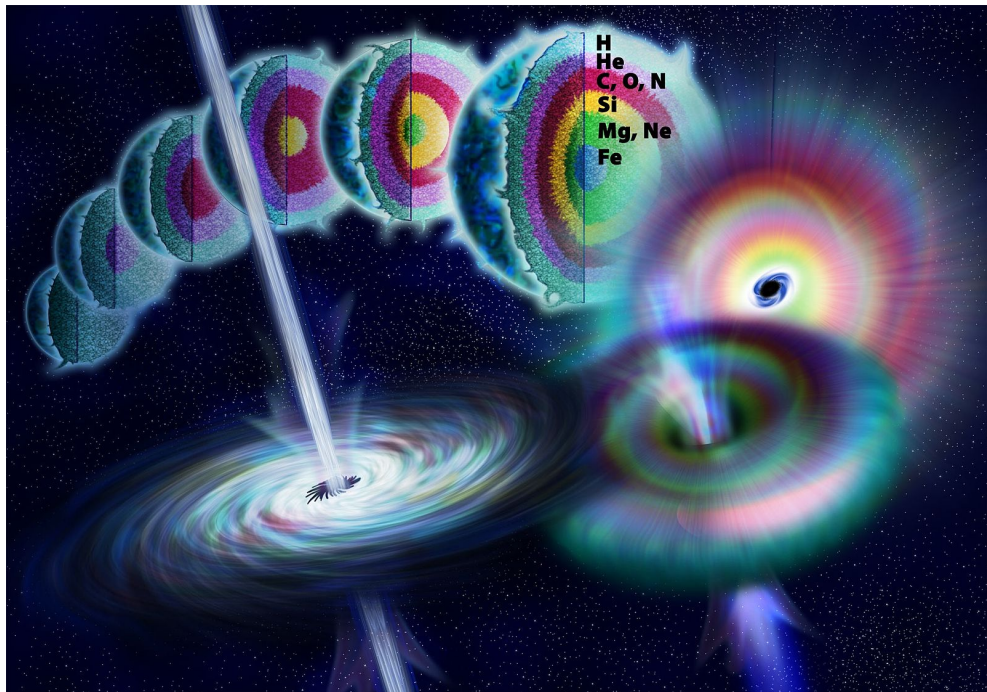


Figure 1.1: The life cycle of a massive star. When fusion stops the collapsing star releases energy in the form of jets observed as a gamma-ray burst

One of the most accepted theories describe GRBs as collisions of highly relativistic outflow of the accelerated jetted matter [10]. For most of the observed GRBs the prompt γ -ray emission was followed by longer-lasting afterglow in soft

X-ray, optical or radio waves [11]. This is due to the propagation of a relativistic shockwave through the medium that surrounds the burst. Observations proved that GRBs are at cosmological distances [12]. The farthest GRB observed was at a distance of $z=9.4$. The average short GRBs lie at a distance of $z=0.5$. The long GRBs are even farther away, on average at $z=2$. The energy that is released is tremendous, about 10 erg. Long GRBs have been linked to the brightest regions of galaxies that contain the most massive stars [13].

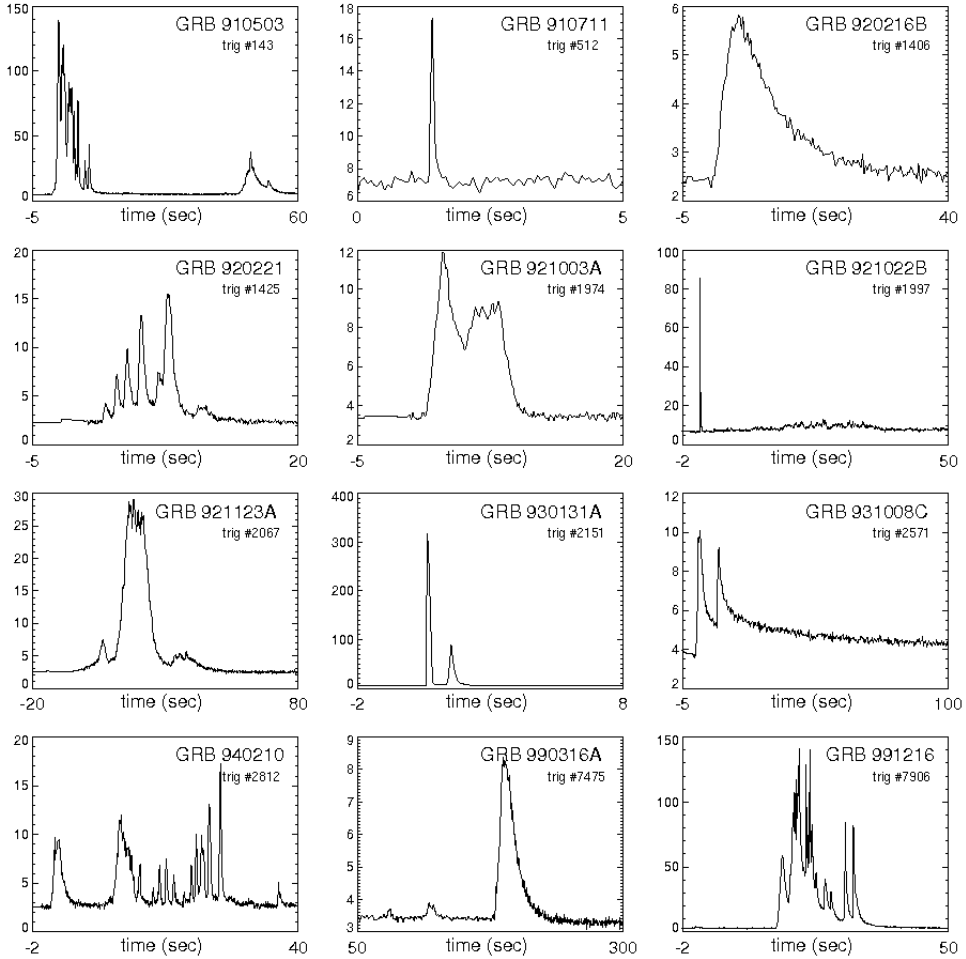


Figure 1.2: The light curves of 12 gamma-ray bursts observed by BATSE. The diversity of the curves is extraordinary. Events with a length from millisecond to a second exist either with smooth or highly variable curves.

On the contrary, short GRBs are thought to originate in old populations. The theory that they originate from the merging of two neutron stars has been recently confirmed by detecting the gravitational waves of such an event. This was detected by the LIGO/Virgo collaboration in 2017 [14]. The electromagnetic counterpart of this gravitational wave event was detected as a short GRB by the Fermi/Gamma-ray Burst Monitor (GBM) and INTEGRAL instruments followed by the observation of the GRB's afterglow and its host galaxy [15]. Short GRBs emit electromagnetic radiation due to the radioactive decay of heavy r-process nuclei that are produced

and ejected almost isotropically during the merger process [16].

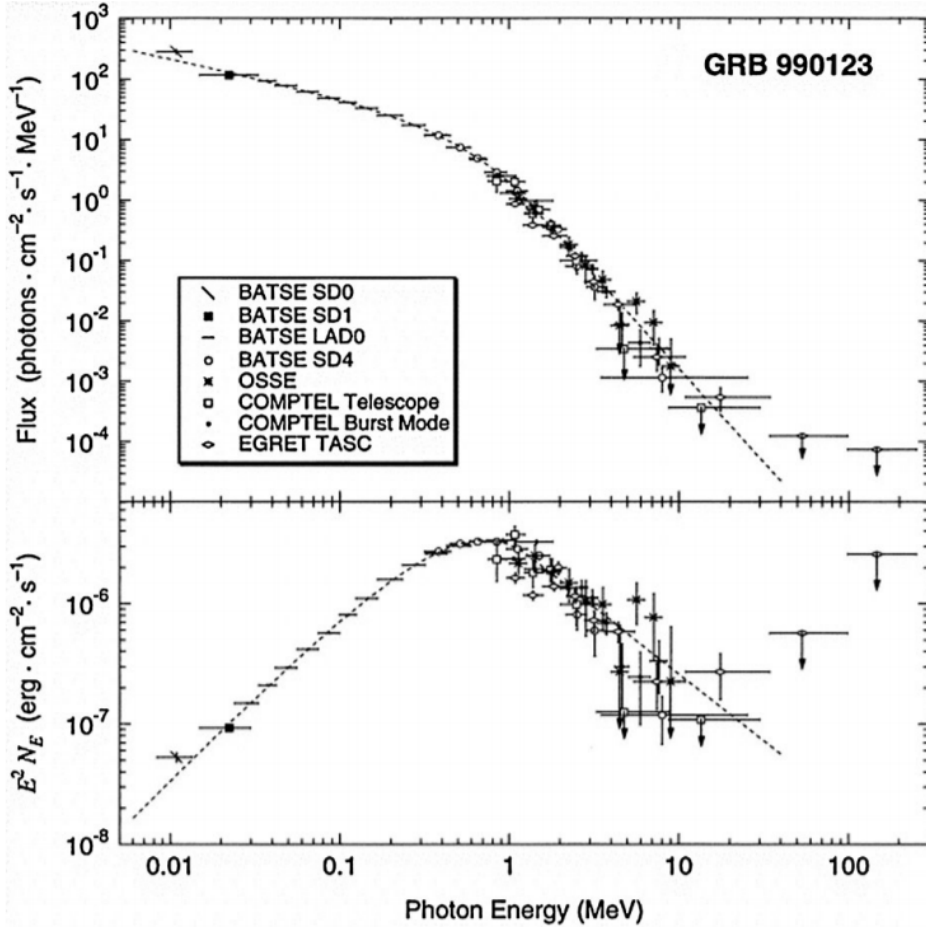


Figure 1.3: The band function of GRB 990123 [43]

Open questions on gamma-ray bursts

Despite the fact that GRBs have been studied for more than forty years a lot of questions are still not understood about their physics[17]. In the following the main open questions are listed:

- Classification: some of the observed light curves can not be classified into short and long GRBs, such as the ultra-long GRBs.
- Central engine: in most cases it is thought that a black hole is formed after the merging of neutron stars and core collapse of massive stars. Although there are models that predict the birth of a magnetar. The most exotic theories predict the birth of a quark star that has never yet been observed.
- Acceleration mechanism of the jets: How particles are accelerated to a velocity of Lorentz-factor of 300 in the shock waves is not yet understood.
- GRB jet composition: there are two possible driving forces behind the acceleration of jet material. The first one is magnetic field dominated and

the other one is dominated by baryons. As the acceleration of particles is not yet fully understood, it is not known whether protons can be accelerated to ultra-high energies. These could produce Ultra-High Energy Cosmic Rays.

- Radiation mechanism: there are several physical processes that create the γ -ray spectrum of GRBs, that is called the "Band" function. The following three processes are thought to be the main contributors to the spectrum: synchrotron radiation, synchrotron self-compton radiation and Compton up-scattering of thermal photons.
- First stars: different population of stars on average have different masses. Models predict that population III stars end their life with a black hole that has a mass about ten times bigger than population I and II stars. The progenitors of GRBs can be classified into populations by their redshift [18].

Search for the electromagnetic counterparts of gravitational wave events

Multi-messenger astronomy is based on the investigation of astronomical objects with disparate "messengers". It opened a possibility to gather information in different ways to understand astrophysical objects. Until 2017 the three messengers were electromagnetic radiation, cosmic rays and neutrinos. 2017 opened a new era in multi-messenger astronomy as the electromagnetic counterpart of GW signal GW170817 was detected by the LIGO/Virgo collaboration. The source of this signal was the short GRB 170817A [19], a binary neutron star merger [15].

This historical detection occurred on August 17, 2017. The Fermi satellite detected the (short) GRB 170817A, approximately 1.7 s before the detection of the GRB, LIGO-Virgo detector network observed a GW signal GW170817. The origin of this source was a neutron-neutron star merger. The source was localized in a sky region of 28 deg² (with 90 % confidence).

After the detection of the GRB signal, several space and earth based observatories in a wide range of wavelengths started the investigation of the source. The discovery of a bright optical transient linked to the GRB was discovered in NGC 4993. Observatories involved in the investigation included Chandra X-ray Observatory [21], INTEGRAL [20], Swift and Nuclear Spectroscopic Telescope ARray (NuSTAR). A blue kilonova associated with this event was detected [22]. It is important to emphasize that not only neutron-neutron star mergers but neutron star-black hole and black hole-black hole mergers can emit electromagnetic signal [23]. Therefore all short GRBs can be investigated with multi-messenger astronomy in the future. As LIGO is constantly upgrading its detectors, gravitational waves will

be detected more often. An even more sensitive gravitational wave detector is under building called Kamioka Gravitational Wave Detector (KAGRA). First scientific measurements will be taken in the 2020s [24].

Particle detectors in space

Almost all types of detectors starting from semiconductor based detectors to gas-filled detectors have been used in space. In the case of search for GRBs the detection of x-rays is the most relevant. Several types of detectors can be used for detecting γ photons[27], for example the semiconductor based German Position Sensitive Proportional Counters (PSPC) of the ROSAT X-ray telescope. For our satellite the size of the detector is limited, therefore the best option was the usage of scintillators. Mostly used scintillators in space include inorganic crystal scintillators, for example NaI(Tl) or CsI(Tl), and plastic scintillators. CsI(Tl) was chosen as the detector of the Camelot CubeSat due to it's high light yield.

Current missions observing gamma-ray bursts

This subsection provides an overview of the existing missions that are aimed to detect GRBs. Field of view (FOV) and localization accuracy are chosen to compare them with the Camelot CubeSat. The proposed design of the Camelot satellite has the advantage of a large field of view and a high localization accuracy. The main idea is that each CubeSat will detect GRBs at the same time. By measuring the time difference between the triggering of each satellite, the GRB source can be triangulated. By using more satellites, the field of view will be the full-sky and localization accuracy increases.

The planned localization accuracy is more precise than any other existing GRB mission, that might reach $\sim 10'$. While providing the highest localization accuracy, the field of view would also be the highest, even larger than the field of view of the INTEGRAL/SPI-ACS and Fermi.

The size and mass of the Camelot CubeSat is less than 1% of the Fermi telescope. Therefore from a fraction of the cost several satellites could be built and deployed in orbit. Having several satellites also provide a high redundancy.

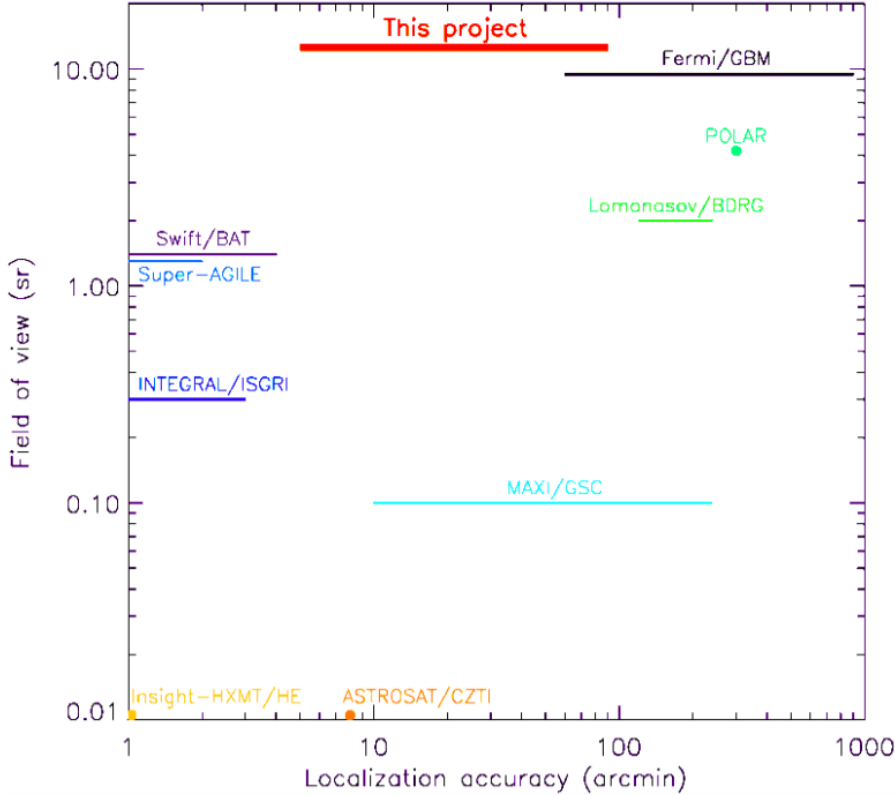


Figure 1.4: The field of view and localization accuracy of several missions including the Camelot CubeSat.

The following list includes the most relevant, currently ongoing missions looking for GRBs:

- Fermi 7 [26] was launched in 2008 and its main instruments are Gamma-ray Burst Monitor and the Large Area Telescope (LAT).
- Neil Gehrels Swift Observatory (Swift) 8 [28] was launched in 2005 and its main instruments are Burst Alert Telescope (BAT), X-ray Telescope (XRT), and UV/Optical Telescope (UVOT).
- INTErnational Gamma-Ray Astrophysics Laboratory (INTEGRAL) 9 [29] was launched in 2002. The most succesfull instruments on board include are the Anti-Coincidence Shield of the SPectrometer of INTEGRAL (SPI-ACS) and the Integral Soft Gamma-Ray Imager (ISGRI) detector layer of the "Imager on Board the Integral Satellite (IBIS)" detector.
- Astro-Rivelatore Gamma a Immagini Leggero (AGILE) 11 [30] was launched in 2007 and its Hard X-ray Imaging Detector (Super-AGILE) detected several GRBs.
- CALorimetric Electron Telescope (CALET) 12 [31] / Gamma-Ray Burst

Monitor (CGBM), was launched in 2015 and it is placed on the International Space Station (ISS).

- Monitor of All-sky X-ray Image (MAXI) 13 [32], started nominal observation in 2009. Its instrument Gas Slit Camera (GSC) detects GRBs. The instrument is placed on ISS.
- Gamma-ray Burst Polarimeter POLAR 14 [33], was launched in 2016 and is dedicated to the measurement of GRB polarization.
- Lomonosov 15 /BDRG [34], was launched in 2016. The BDRG instrument on board detected several GRBs.
- The Hard X-ray Modulation Telescope (Insight-HXMT) 16 [35], was launched in 2017. It has on board the high energy X-ray telescope (HE), the medium energy X-ray telescope, and the low energy X-ray telescope.
- ASTROSAT 17 [36], was launched in 2015 and its Cadmium Zinc Telluride Imager (CZTI) has already detected many GRBs.
- Reuven Ramaty High Energy Solar Spectroscopic Imager (RHESSI) 18 [37], was launched in 2002. It is designed to study hard x-ray and gamma-ray emission from solar flares, however it is also efficient instrument to detect non-solar gamma-ray events like GRBs.

The CAMELOT satellite

There would most likely be four scintillators on the CAMELOT satellite. On two neighbouring sides of the satellite have two scintillators each. The scintillator will have a case either from aluminium or carbon fibre.

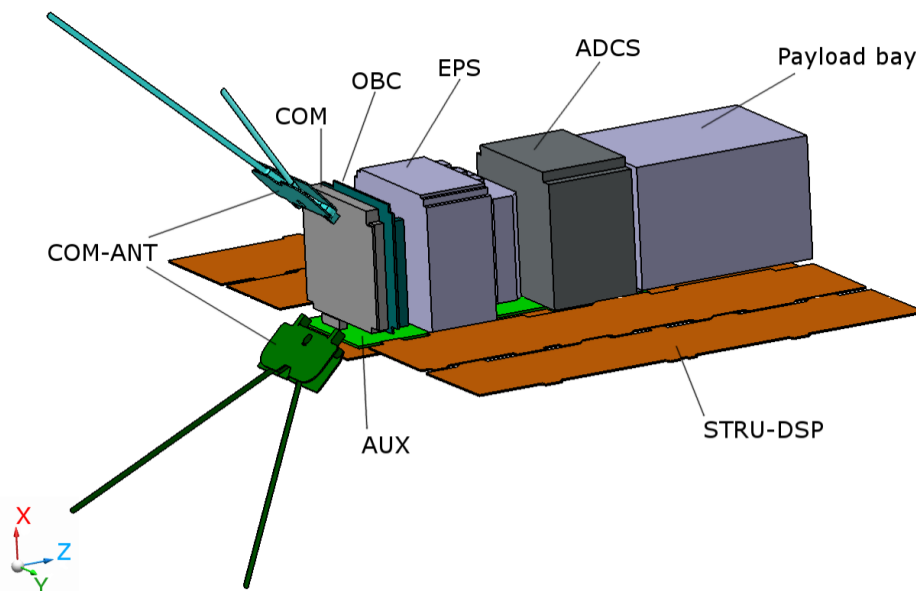


Figure 1.5: The modules of the satellite

The Camelot satellite will consist of the following modules:

- On-Board Computer [OBC] is responsible for control all the satellite's sub-systems. OBC collects housekeeping and payload data and archives them in its internal storage.
- Electrical Power System [EPS] is responsible for managing primary and secondary power sources and distributing power at appropriate voltage levels to on-board subsystems.
- COM UHF Transceiver [COM] provides an RF communication link between the Ground Segment and the satellite. The COM codes the received messages from the OBC and transmits to the Ground Segment. Furthermore, the COM decodes the received RF messages from the Ground Segment and transmits to the OBC.
- Attitude Determination and Control System [ADCS] determines and controls the satellite attitude.
- Auxiliary Electronics [AUX] subsystems control the deploying mechanisms and monitor the solar arrays. The Aux subsystem also contains the rigid backplane of the satellite; therefore, it also connects the subsystems.
- Structure [STRU]
- Ground Support Equipment [EGSE]

The detection of GRBs

In the case of our satellite, the detection of γ photons from GRBs will be carried out by a Caesium Iodide scintillator doped with Tellurium. This is the most popular alkali halide scintillation crystal apart from NaI(Tl). The γ photons create scintillation, thus thousands of optical photons in the scintillator. These photons will be detected by Silicon Photomultiplier device called Multi Pixel Photon Counter, MPPC for short. This is by far the best and most compact solution as the size of cubesat standard is limited to be $\sim 300 \times 75 \times 5 \text{ mm}^3$. The first tests were carried out by a single MPPC readout, which was followed by a design with two MPPCs to maximize the light yield and minimize the noise. The size of the Hamamatsu MPPC is $6 \times 6 \text{ mm}^2$. The scintillators will be placed onto the surface of the satellite as can be seen in fig. 1.6. While fig. ?? shows the experimental setup used for the tests.

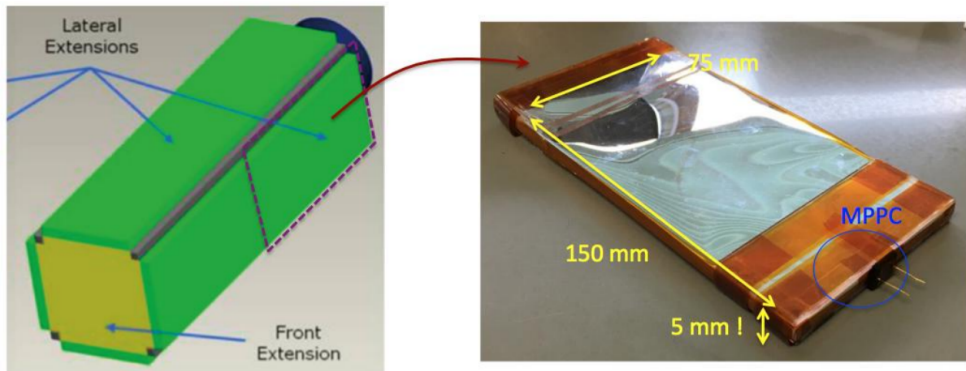


Figure 1.6: Side extensions including of the CAMELOT satellite (left) where scintillators are placed and and a wrapped scintillator with the MPPC read out (right)

The large area and small thickness of the scintillator makes it challenging for the read out as optical photons have to be reflected several times to reach the MPPC. Two factors play role here, the self absorption of the reflectivity of the tape that is used to cover the scintillator. The length of the self absorption is in the order of a meter and the reflectivity of the ESR tape, which is above 99 % can be seen in fig. 1.10. The idea that we came up with is using two MPPC-s with coincidence. This results in a smaller leakage current (noise) as the noise has a poissonian statistic. Therefore the noise is "random" and the chance of a trigger from both of the MPPC has a very low chance. The other advantage is the increased photon yield due to the double of the photon collection area. The difference between one and two channel readout can be seen in fig. 1.7.

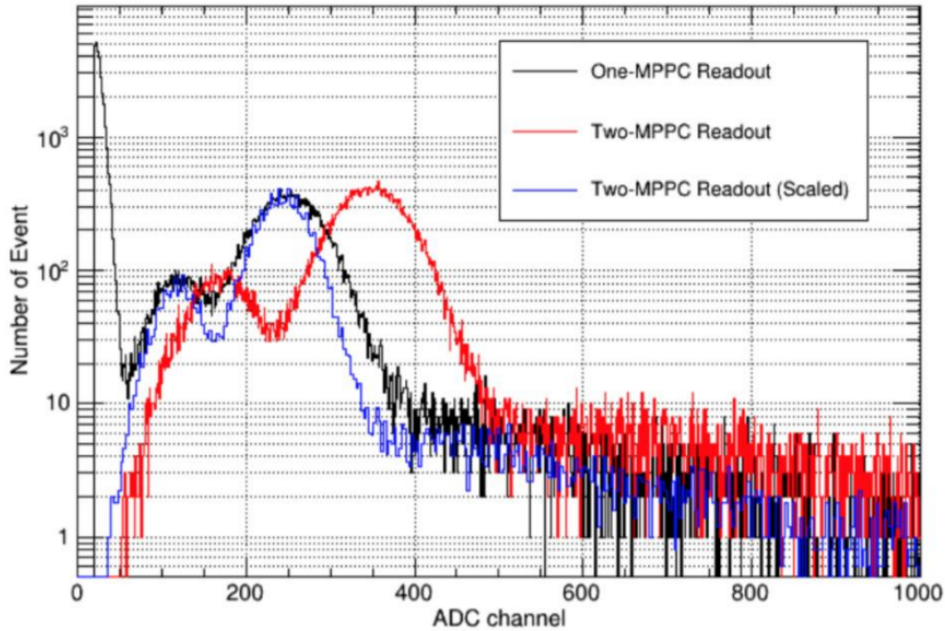


Figure 1.7: Energy spectra obtained by collecting the signal of 1 million γ with the one channel and the two channel read out

The Geant4 platform

The most used software in particle physics are MCNPX, FLUKA and Geant4. For this thesis Geant4 was chosen as it is the best for simulation of several types of particles at the same time and building up the geometry of detectors is most probably is the most convinient in the software.

Geant4 [44, 45, 46] (for GEometry ANd Tracking) is a platform for "the simulation of the passage of particles through matter," using the Monte Carlo method. It has been developed at CERN for more than three decades by dozens of physicists and programmers. The cross sections for all interactions between matter and particles are included in this software. It is an object orientated programming platform in C++. Its development, maintenance and user support are taken care by the international Geant4 Collaboration. Areas in science that has used Geant4 are very wide from the design of complex medical machines to accelerator, nuclear physics, hight energy physics and space applications. Several thousand people use it all around the globe.

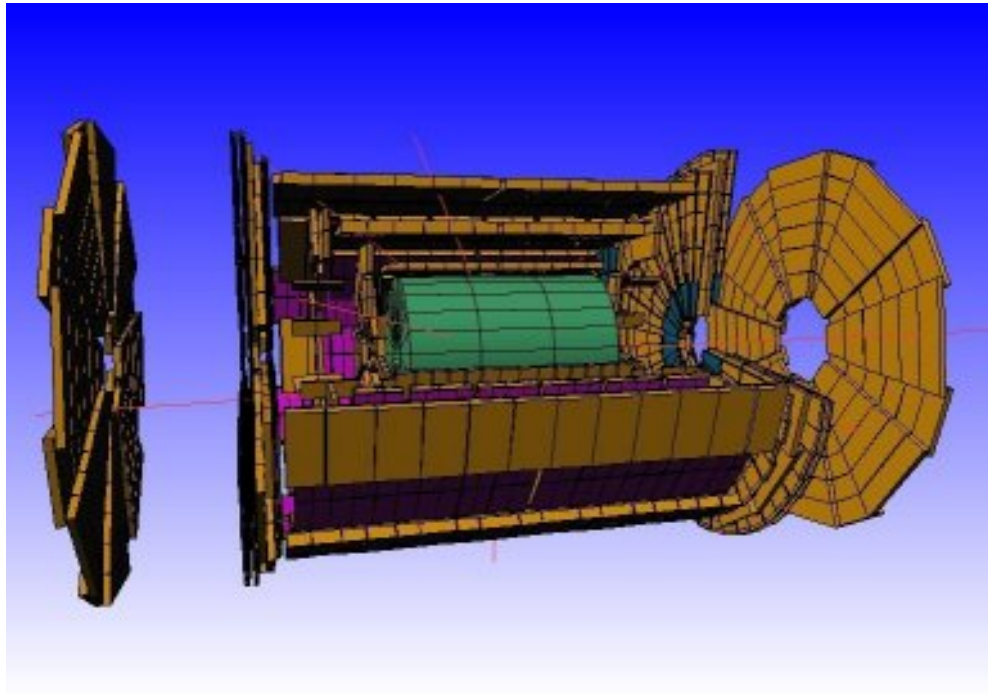


Figure 1.8: The Geant4 simulation of the whole ATLAS experiment

The Geant4 platform includes all the important features required in the full simulation of an experiment from handling the geometry of the detector and readout, tracking of particles in the detectors for visualization.

The experimental setup

In order to understand and characterize the behaviour of the large-area CsI(Tl) scintillator detector and the MPPC readout an experimental setup was built in Hiroshima, Japan. The experimental setup provided vital information for the simulation, mostly for the position dependence of the light yield. Different γ source were used, mostly an ^{241}Am source.

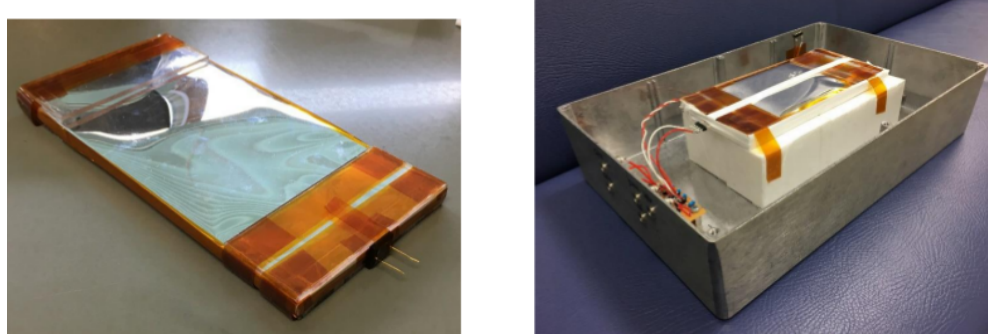


Figure 1.9: The scintillator on the left and the cage holding the setup on the right

The detector was wrapped in a so called ESR foil that is designed to reflect as much light as possible. In fig. 1.10 the reflectivity of this tape can be seen depending on the wavelength of the photons, exceeding 99 % for most of the wavelengths. It is

important as the optical photons have to be reflected several times in order to be read out with the small effective area of the MPPC. This reflectivity was included in the simulation.

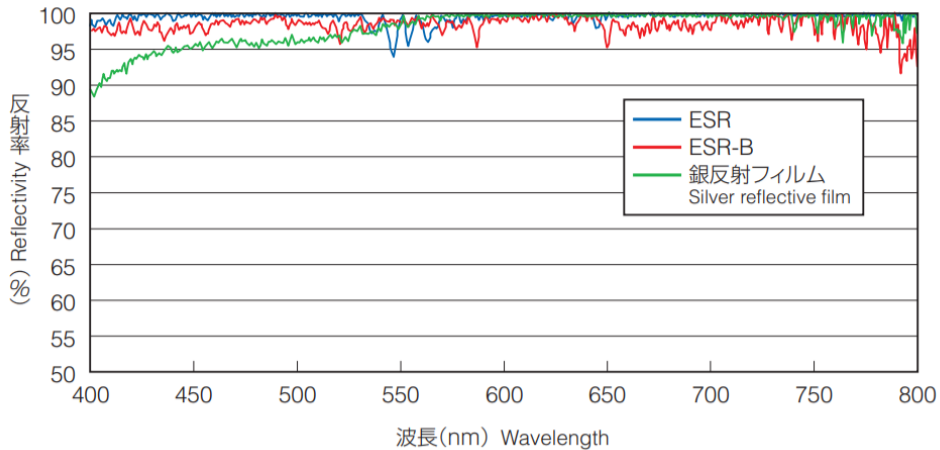


Figure 1.10: The reflectivity [50] of the ESR tape that was used to wrap the scintillator in order to increase the light yield. This data was included in the simulation.

The CsI(Tl) scintillator used is produced by AmCrys [50]. The dimension of this detector are 150 mm x 75 mm x 5 mm, the largest possible size that can fit onto the surface of the detector. The spectra of the optical photons produced in the scintillation process can be seen in fig. 1.11. An aluminium case of 2mm is used, the same as planned for the mission in space. The time constant for the scintillation of the detector was 200 ns.

Energy [eV]	3.54	3.10	2.76	2.48	2.36	2.25	2.07	1.91
Relative emittance	0.02	0.1	0.3	0.6	0.9	1.0	0.7	0.4
Refractive index	1.59	1.57	1.54	1.54	1.54	1.54	1.54	1.54
Absorption length [cm]	50	50	50	50	50	50	50	50

Table 1: The parameters of the CsI(Tl) scintillator used in our experiment

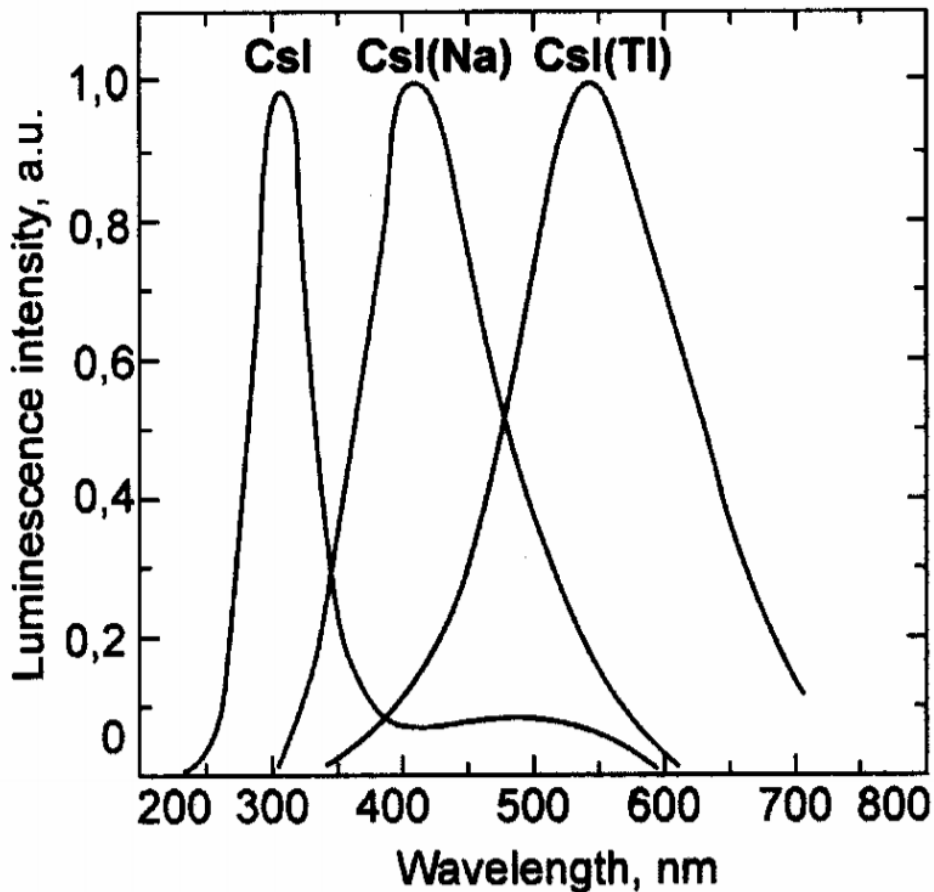


Figure 1.11: The emitted scintillation light spectra of three types of scintillators. In our experiment CsI(Tl) was used

The MPPC chosen for this satellite is one of the latest models (HAMAMATSU S13360-6050CS) [51]. It has an effective area of 6mm x 6mm. The photon detection efficiency of this specific model can be seen in fig. 1.12.

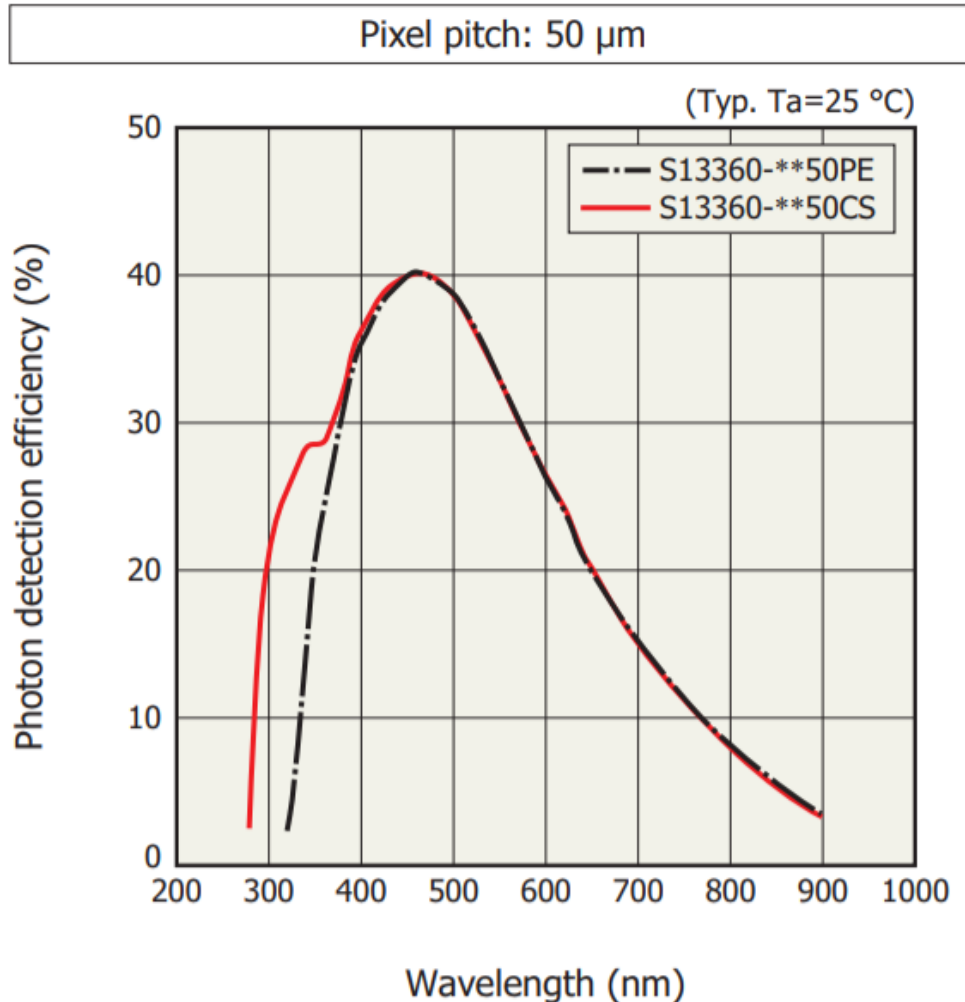


Figure 1.12: The photon detection efficiency [51] of the MPPCs used for the readout of the scintillators. This data was included in the simulation.

The readout of the detector

The response of the MPPC detector used depends on temperature. Therefore the experimental setup was placed in a thermostatically controlled chamber (ESPEC LU-113) keeping the temperature at 25°. Two setups were investigated. The first one with a single MPPC readout placed in the middle of one side of the scintillator. In the other case two MPPCs were utilized symmetrically placed on one side of the detector.

For the single MPPC readout setup a commercial charge-sensitive preamplifier (CLEAR-PULSE 5028), a shaping amplifier (EG&G ORTEC 571), and an ADC (AMPTEC MCA800A) were used to obtain an electric signal read out by a PC. The shaping times was set to 1 μ s.

For the case of the two-channel read out an FADC board was utilized that contains all the necessary electronics to read out the signal of the MPPC with an additional coincidence unit. This board was developed for the astrophysical

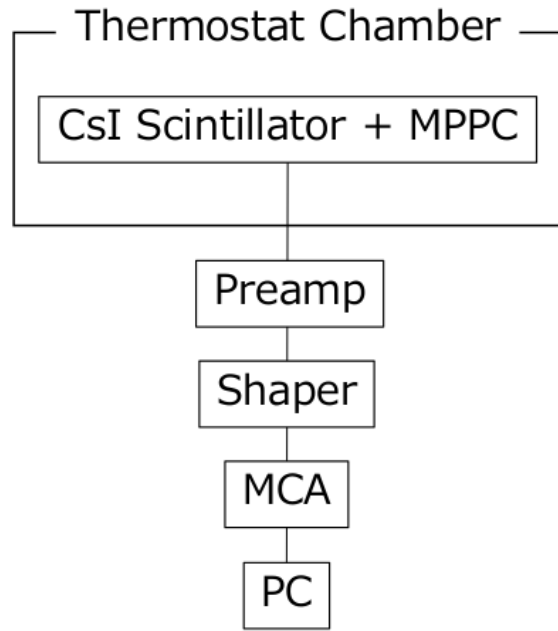


Figure 1.13: The schematic design of the readout of the MPPC for the 1 channel configuration

polarimetry mission PoGO+. The shaping time was set to $2.2 \mu\text{s}$ in this case. The breakdown voltages of the two-MPPCs are almost the same—50.82 and 50.87 V—at 25 C. We used a KEITHLEY 2400 to supply the operational voltage of 53.4 V.

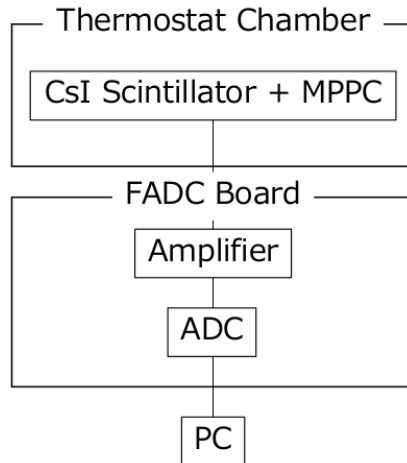


Figure 1.14: The schematic design of the readout electronics of the 2 channel setup

1 channel setup

The γ source that was used to test the experimental setup was chosen to be an ^{241}Am . The reason for this is that the peak of energy spectrum of the γ photons from GRBs is at 50 keV which is very close to the peak of the ^{241}Am that is 59.5 keV. The activity of the source at the time of the experiment was 471 kBq. The source was collimated to a beam that hit the surface of the scintillator on a circle with a radius of 10 mm. The distance of the source from the scintillator was 13.5 mm.

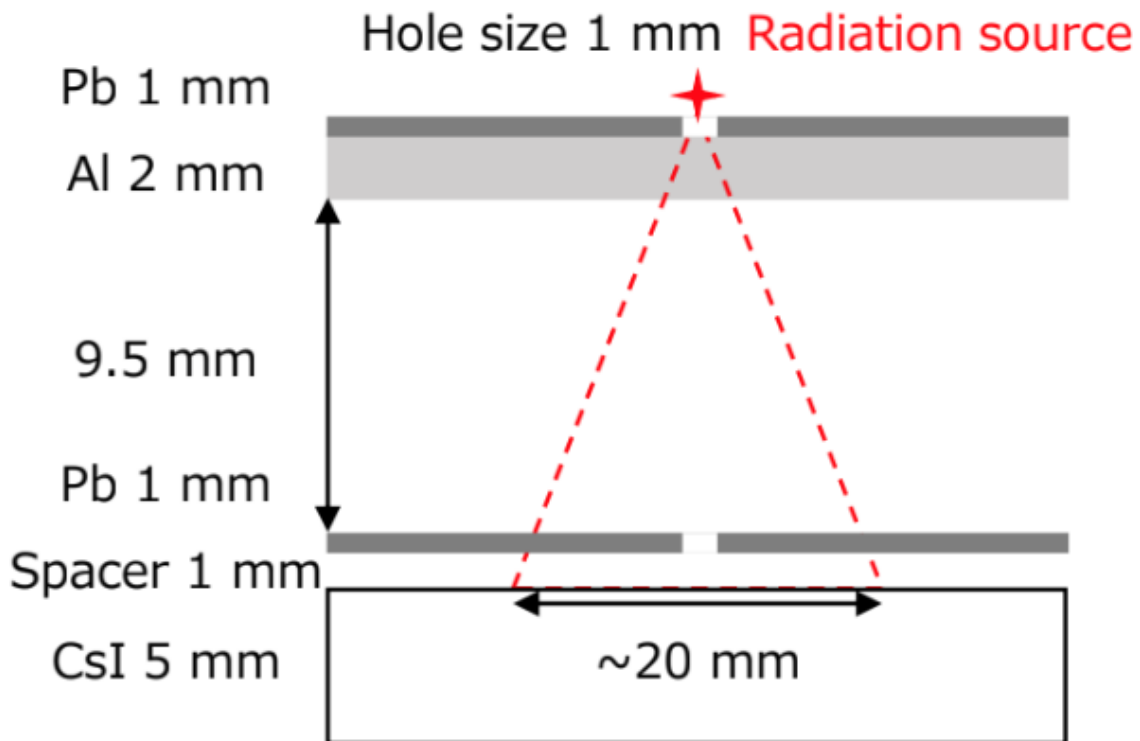


Figure 1.15: The ^{241}Am gamma source was placed in a collimator system as can be seen on the image

Therefore the solid angle of the part of the whole sphere where γ s could be detected was

$$\Theta = 2\pi(1 - \cos(\theta)) = 1.234\text{sr}$$

2 channel read out setup

In order to maximize the light yield, thus the signal of the detector and minimize the noise with coincidence a 2 channel setup was tested. In fig. 1.16 this setup can be seen with the MPPCs placed symmetrically to the scintillator.

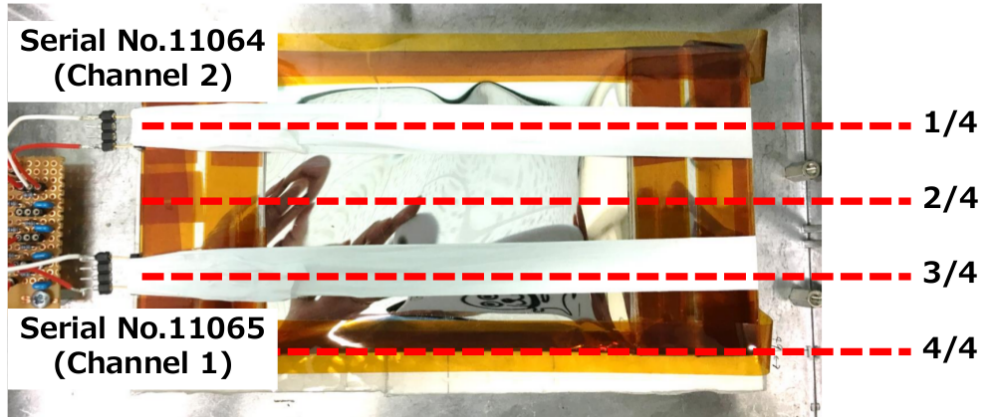


Figure 1.16: The MPPCs for the 2 channel readout are positioned symmetrically from the center of the scintillator

The geometry of the two channel read out setup was simulated

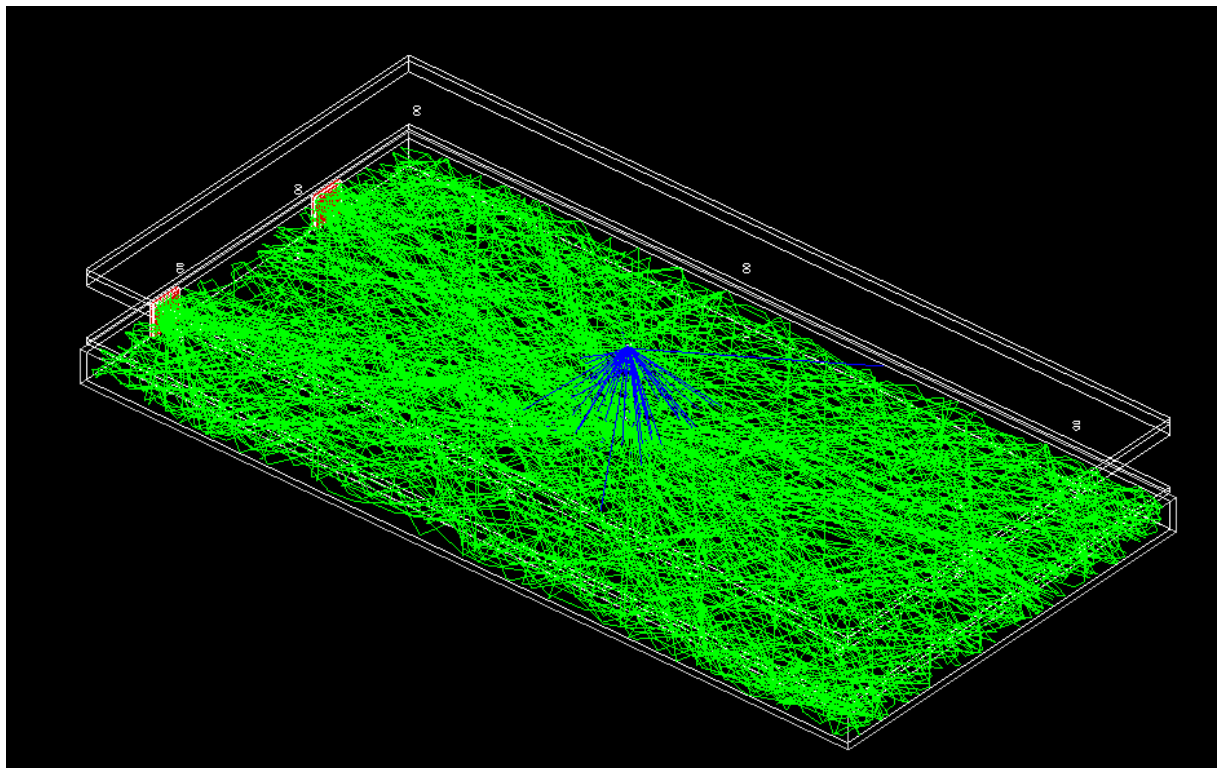


Figure 1.17: Simulation of 100 γ s emitted from the source. The blue lines represent the track of the γ s and the green lines represent the track of the optical photons created by scintillation. Only the photons that were detected are drawn.

The satellite

The direction of GRBs is isotropic in the sky as they are extragalactic objects. As the positioning of the scintillators is not decided yet it is important to understand which configuration would be the best for detecting as many GRBs as possible. Therefore it is vital to understand how the material of the satellite itself absorbs γ s. The satellite consists of several modules with specific shapes and material contents. Therefore building up the whole geometry and material composition was not possible in Geant4, thus the model of the satellite had to be imported into Geant4.

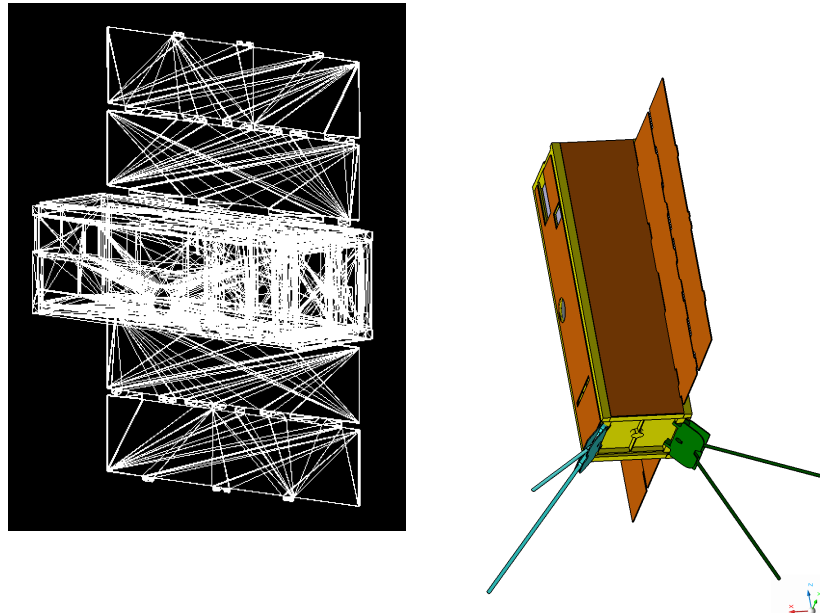


Figure 1.18: The CAD model of the satellite (on the right) and the view of the imported model in Geant (on the left)

Importing predefined CAD models into GEANT4 is not always possible or requires intermediate file format conversion to Geometry Description Markup Language (GDML) using commercial or third party software. CADMesh [47] is a direct CAD model import interface for GEANT4 leveraging ASSIMP [48] for reading the CAD files. In this work the CAD model of the satellite was exported to STL files. These files were imported by the CADMesh software to Geant4. The tessellation was done by the TETGEN [49] software.

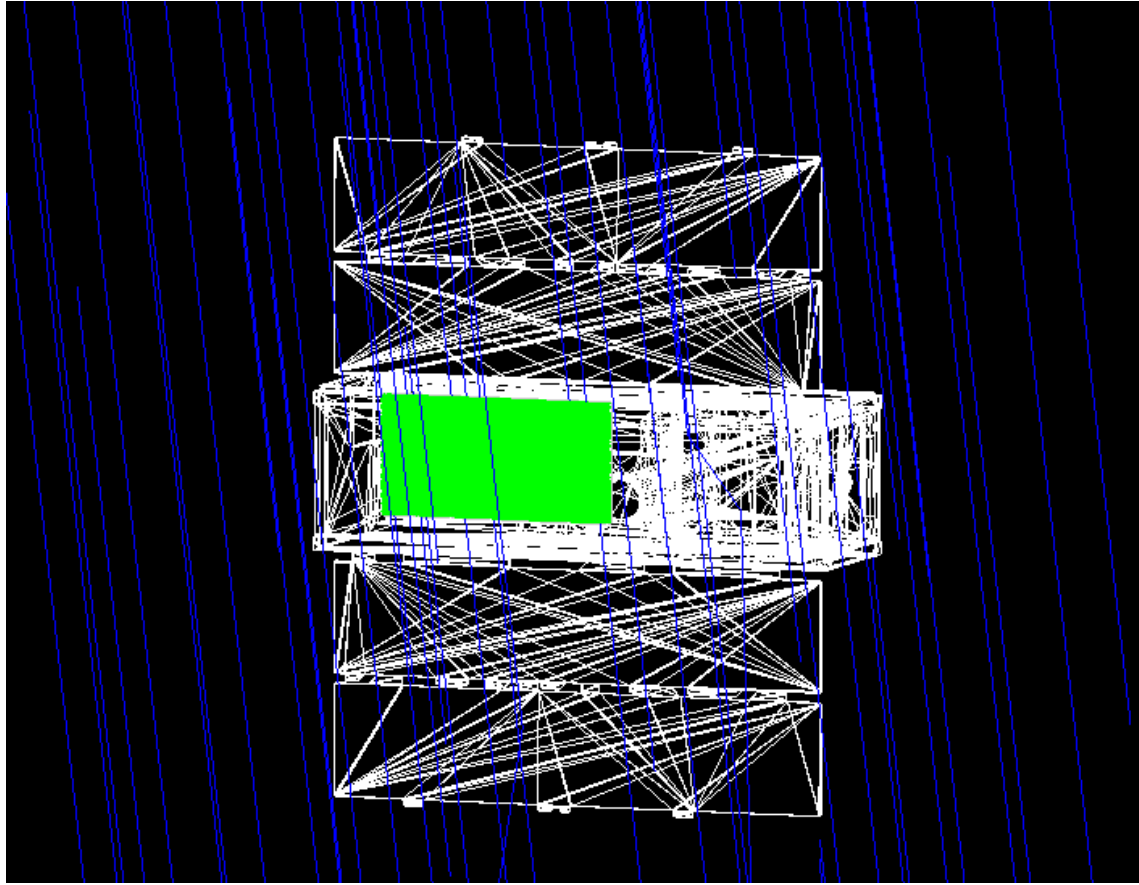


Figure 1.19: The satellite radiated by a pencil beam of 10.000 γ particles. The scattered γ s induce signal in the scintillator

Name of module	mass [g]	Type of material	Mass ratio [%]
ADCS	710	Aluminum 6061-T6	50
		Copper Electric	25
		Glass Borosilicate	25
COM	90	Stainless Steel	2
		Brass Generic	25
		Aluminum 7075-T73	40
		FR4 Glass-Epoxy sheet	33
EPS	750	FR4 Glass-Epoxy sheet	25
		Aluminum 6061-T6	75
OBC	50	FR4 Glass-Epoxy sheet	100
STRU	980	Aluminum 6061-T6	100
SP	570	Solar Panel	100
Payload	1100	As you wish	100

Table 2: The mass ratio of materials that are used for the satellite

Results of the simulation

Comparison of the results of the simulation with experiments

Material name											
Aluminum 6061-T6	Al	96.90	Mg	1.20	Si	0.80	Fe	0.70	Cu	0.40	
Aluminum 7075-T73	Al	88.60	Zn	6.10	Mg	2.90	Cu	2.00	Si	0.40	
Stainless Steel	Fe	66.50	Cr	20.00	Ni	10.50	Mn	2.00	Si	1.00	
Copper Electric	Cu	100.00									
Glass Borosilicate	Si	42.10	O	54.80	B	3.10					
FR4 Glass-Epoxy	Si	23.39	O	36.02	C	37.04	H	3.55			
Brass Generic	Cu	85.00	Zn	15.00							
Solar Panel	Ge	38.00	Si	24.00	O	20.00	C	13.00	H	4.00	B
											1.00

Table 3: The chemical composition of materials that are used for the satellite

X-ray fluorescence

The measured spectra of the scintillation light created by γ -rays (fig. ??) has a main peak that corresponds to the 60 keV γ s from the ^{241}Am source. There is an additional peak with an amplitude of roughly 20 % of the main peak. The physical process that is behind this is the X-ray fluorescence. By default this process is not included in the Geant4 simulations, thus I had to turn it on. A histogram with and without x-ray fluorescence can be seen in fig. 2.1

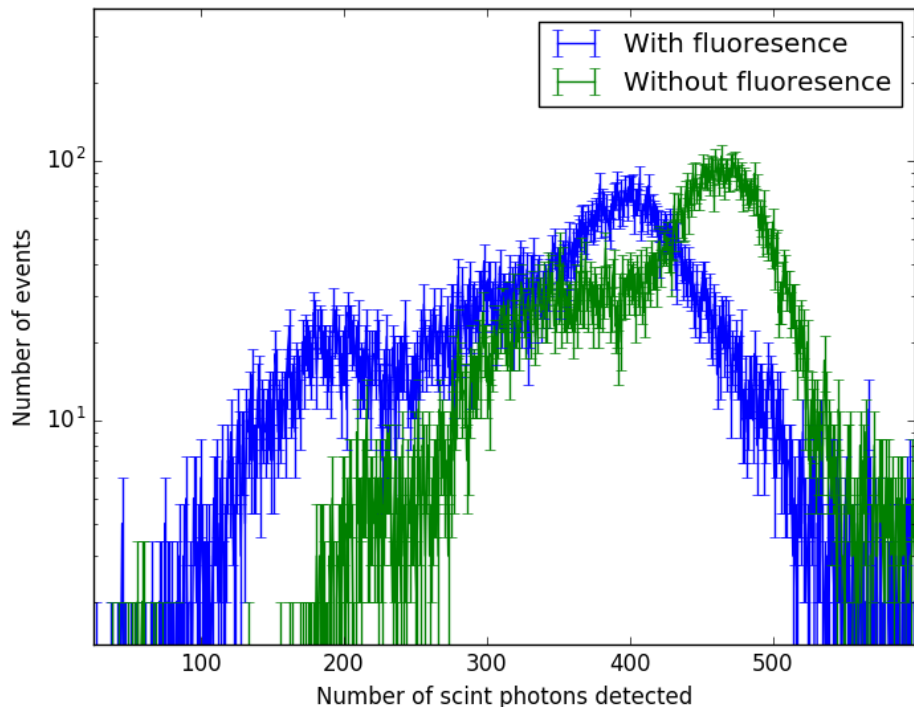


Figure 2.1: The obtained energy spectra from simulation with and without x-ray fluorescence being turned on. One can see that, the first peak, which can be seen in the experiments only appear when x-ray fluorescence was turned on.

Calibration of the position dependence

The main aim of this thesis is to predict what signal the satellite would measure in space. In order to fine tune the parameters of the simulation experimental data was used. The light yield from different parts of the detector is different as scintillation photons have to travel a different distance and they need to be reflected back from the ESR tape that is wrapped around the detector.

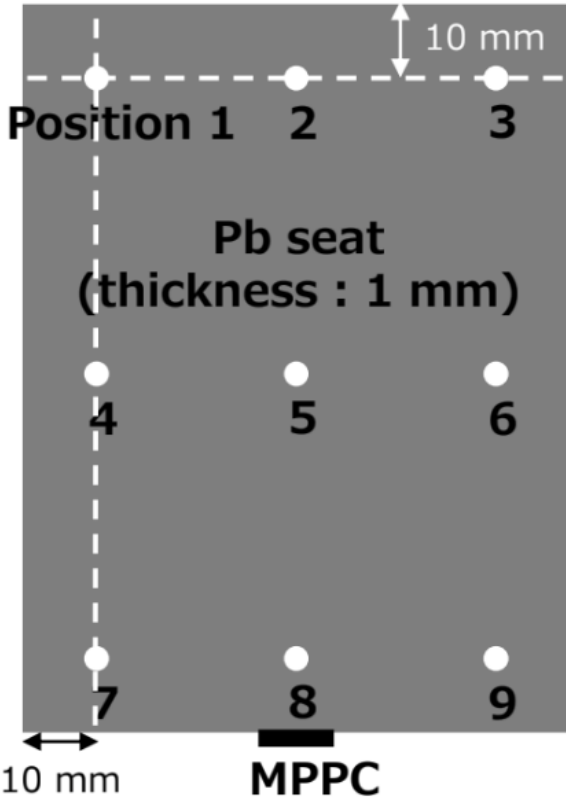


Figure 2.2: The positions of irradiation for the investigation of the response of the scintillator

A lead sheet was drilled with nine holes to collimate the γ source to certain parts of the scintillator. These measurements were carried out by Kento Torigoe at the University of Hiroshima. This configuration with a lead sheet was built up in Geant4 (fig. 1.17 and 3.6 million γ s were simulated at each position).

Pos. of source	1	2	3	4	5	6	7	8	9
Pos. of main peak	0.642	0.664		70.7	0.743		0.598		

Table 4: The position dependence of the photon yield measured at the University of Hiroshima by Kento Torigoe

The three most relevant parameters of the setup in this case are the scintillation photon yield of the scintillator, the reflection rate of the ESR tape and the self-absorption of the scintillator. The photon yield was fixed to 540 keV^{-1} taken

from the data sheet of the scintillator [50]. The self-absorption and the reflection rate was increased until the position dependence was the same as in the experiment (table. 5).

Refl:	0.995	Abs.: 50 cm							
Pos. of source	1	2	3	4	5	6	7	8	9
Pos. of main peak	0.4013	0.3917	0.3981	0.4045	0.4172	0.4140	0.2580	1	0.2739
Refl:	0.997	Abs.: 60 cm							
Pos. of source	1	2	3	4	5	6	7	8	9
Pos. of main peak	0.4588	0.4587	0.4697	0.4734	0.4700	0.4737	0.3388	1	0.3365
Refl:	0.999	Abs.: 80 cm							
Pos. of source	1	2	3	4	5	6	7	8	9
Pos. of main peak								1	
Refl:	0.9996	Abs.: 80 cm							
Pos. of source	1	2	3	4	5	6	7	8	9
Pos. of main peak								1	
Refl:	0.9999	Abs.: 105 cm							
Pos. of source	1	2	3	4	5	6	7	8	9
Pos. of main peak	0.6911	0.6865	0.6956	0.7002	0.6956	0.7002	0.6041	1	0.5955

Table 5: The position of the Gaussian peak fitted to the 60 keV peak of the Am source for several irradiated positions

Calibration of photon yield

In the simulation 3.6 million γ s were simulated. The measurement took 240 s. Therefore the number of photons emitted by the source was ~ 11.0 million. The amplitude of the peaks in the energy spectrum of signal obtained by the MPPC depends mostly on three parameters. The absorption length of the scintillation light in the scintillator, the reflectivity of the surface and the scintillation photon yield of the scintillator. In order to obtain the histogram that we would measure by the MPPC, the histogram obtained by the simulation had to be scaled up both in amplitude and energy. (The introduction of an offset was not needed as the origin point of the histogram obtained in the measurements was shifted to zero energy.)

The energy bins had to be scaled up by a factor of 2.4 to match the experimental results. The amplitude had to be scaled up by a factor of 26.2.

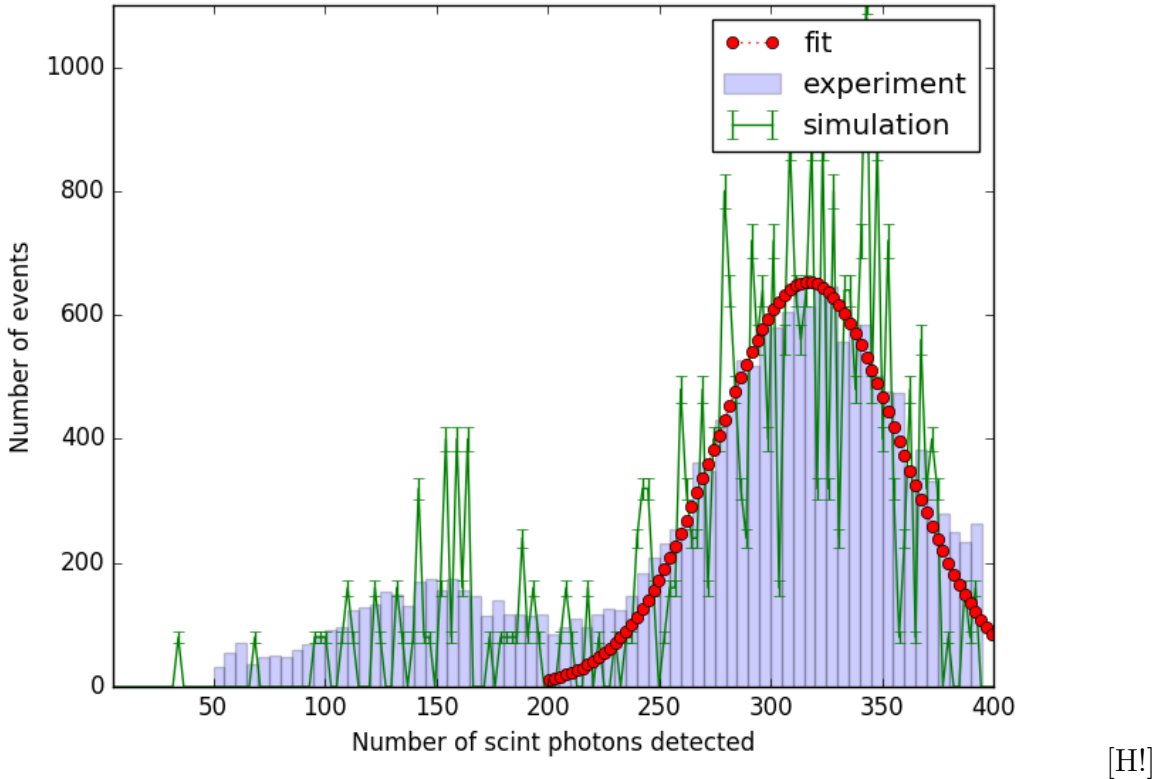


Figure 2.3: The spectra of 11 million photons taken experimentally (blue histogram) matched up with the results of the simulation (green histogram) and the Gaussian fitted to the simulated data

Simulation of the signal induced by GRBs in the satellite

One of the key questions is what would the satellite measure in space when the γ photons of the GRB hit it. It is important to understand how the material of the satellite would absorb the γ photons.

In order to quantify the detection, the number of particles detected was used as a measure. 10.000 γ particles were shot at the detector paralelly on an area of 60cm x 60cm from several angles around the longitudinal axis of the satellite. This way the self absorption of the satellite was quantified.

The energy spectra of γ photons (called band function) from GRBs is fitted by the following equation [53]:

$$f_{BAND}(E) = A \begin{cases} \left(\frac{E}{100 \text{ keV}} \right)^\alpha \exp \left[-\frac{(\alpha+2)E}{E_{peak}} \right] & E \geq \frac{(\alpha-\beta) E_{peak}}{\alpha+2} \\ \left(\frac{E}{100 \text{ keV}} \right)^\beta \exp(\beta - \alpha) \left[\frac{(\alpha-\beta)E_{peak}}{100 \text{ keV} (\alpha+2)} \right]^{\alpha-\beta} & E < \frac{(\alpha-\beta) E_{peak}}{\alpha+2} \end{cases}$$

where the parameters of the fit are following for GRB 990123:

$$\alpha = -0.87 \pm 0.01$$

$$\beta = -2.9 \pm 0.11$$

$$E_{peak} = (617 \pm 7.09) keV$$

$$A = (0.0262 \pm 0.0000993) s^{-1} cm^{-1} keV^{-1}$$

Simulation of the cosmic background in space

In order to understand what would give the measured background of the satellites, cosmic and solar protons and electrons were simulated in the same way as the γ particles were in sec. 2.2. The flux of and energy distribution of protons and electrons vary widely in the lower orbits around Earth due to its magnetic field. The SPENVIS [54] information system was used to obtain the proton and electron energy spectra.

SPENVIS is ESA's SSpace ENVironment Information System, a WWW interface to models of the space environment and its effects; including cosmic rays, natural radiation belts, solar energetic particles, plasmas, gases, and "micro-particles".

Proton background

500km_protons_max.txt 13535.1 minimum 12076.5

In order to include the resonances in the cross section of the hadron-hadron interactions, additional physics models are needed to be included in the simulation. The signal induced by these resonances might affect the measurement of the protons.

The AE-8 model was used in SPENVIS to obtain the spatially avaraged proton energy spectra for an altitude of 500 km both for solar minimum and maximum. The inclination of the orbit was chosen to be 89° . At the moment hadron resonances are not taken into account in the simulation.

In order to include the resonances in the cross section of the hadron-hadron interactions, additional physics models are needed to be included in the simulation. The signal induced by these resonances might affect the measurement of the protons.

Electron background

500km_electrons_min.txt 1.19384e+06 500km_electrons 2.69537e+06

Electrons 'Trapped electron model: AE-8 MIN'

The AE-8 model was used in SPENVIS to obtain the spatially avaraged elextron energy spectra for an altitude of 500 km both for solar minimum and maximum. The inclination of the orbit was chosen to be 89° . At the moment hadron resonances are not taken into account in the simulation.

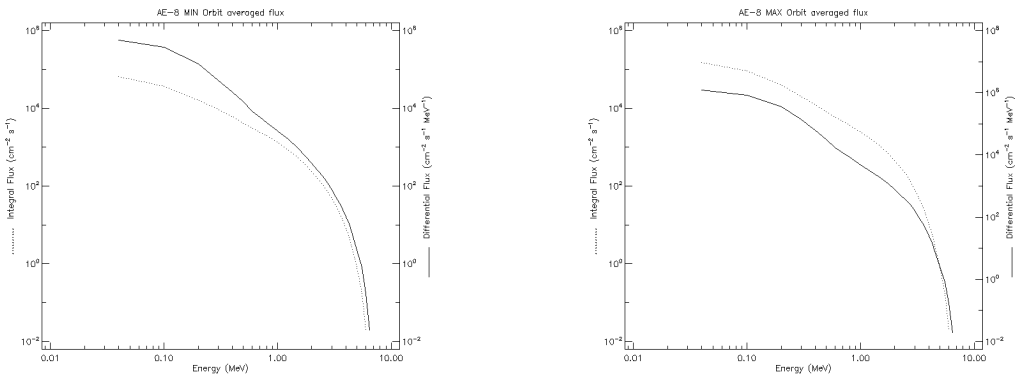


Figure 2.4: The spatially avaraged band function (differential flux for a given energy band, solid line) and the integrated band function (dotted line) of electrons at an altitude of 500 km for solar minimum (left) and solar maximum (right)

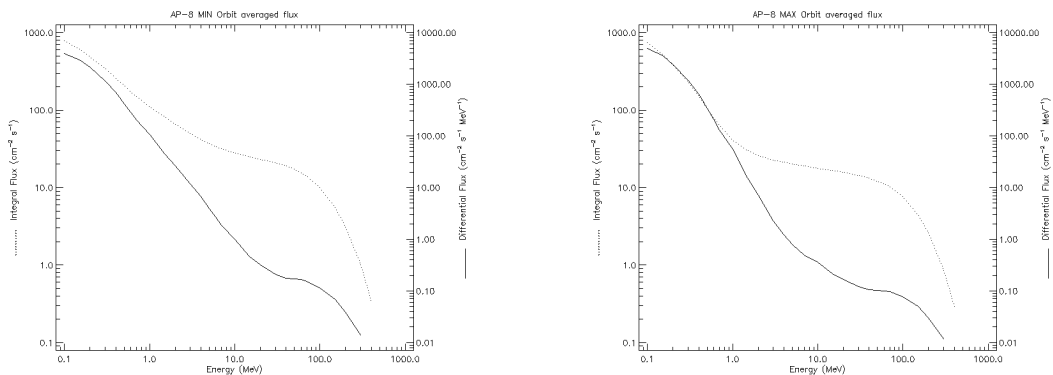


Figure 2.5: The spatially avaraged band function (differential flux for a given energy band, solid line) and the integrated band function (dotted line) of protons at an altitude of 500 km for solar minimum (left) and solar maximum (right)

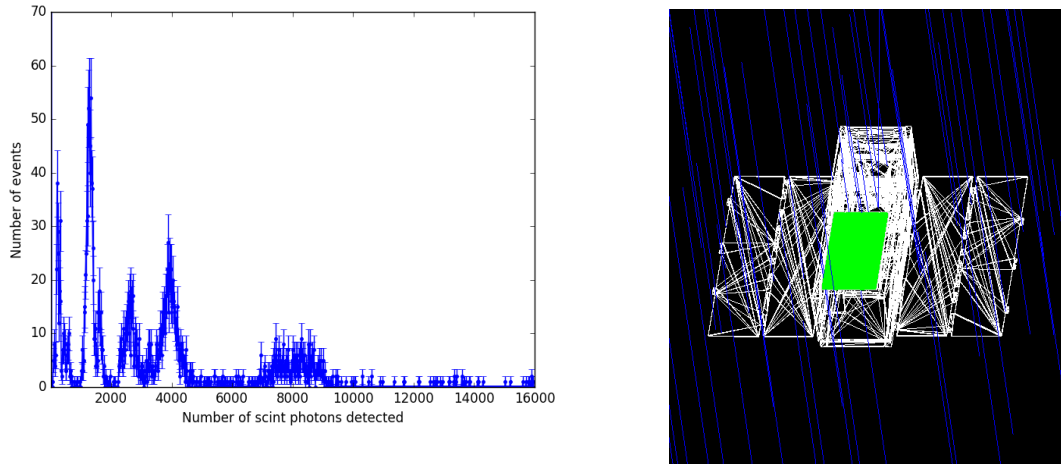


Figure 2.6: The spectrum measured when the electrons were shot perpendicular to the scintillator (called angle of 0°)

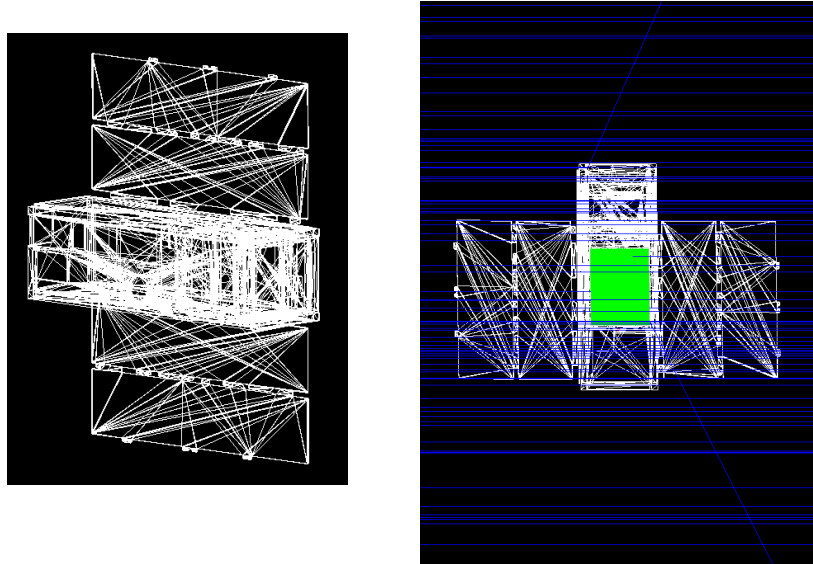


Figure 2.7: The CAD model of the satellite (on the right) and the view of the imported model in Geant (on the left)

Conclusion

In order to simulate how the Camelot CubeSat would interact with the cosmic background and how sensitive it would be to GRBs that it is designed to investigate a Geant4 simulation was built.

As the first step, the experimental setup that was used to test the CsI(Tl) scintillator – the particle detector of the satellite – was implemented in Geant4. The optical parameters of the simulation were fine tuned by comparing the light yield of the MPPCs that was used to read out the scintillator. After the calibration, the results of the simulation was capable of predicting the signal that would be measured in space.

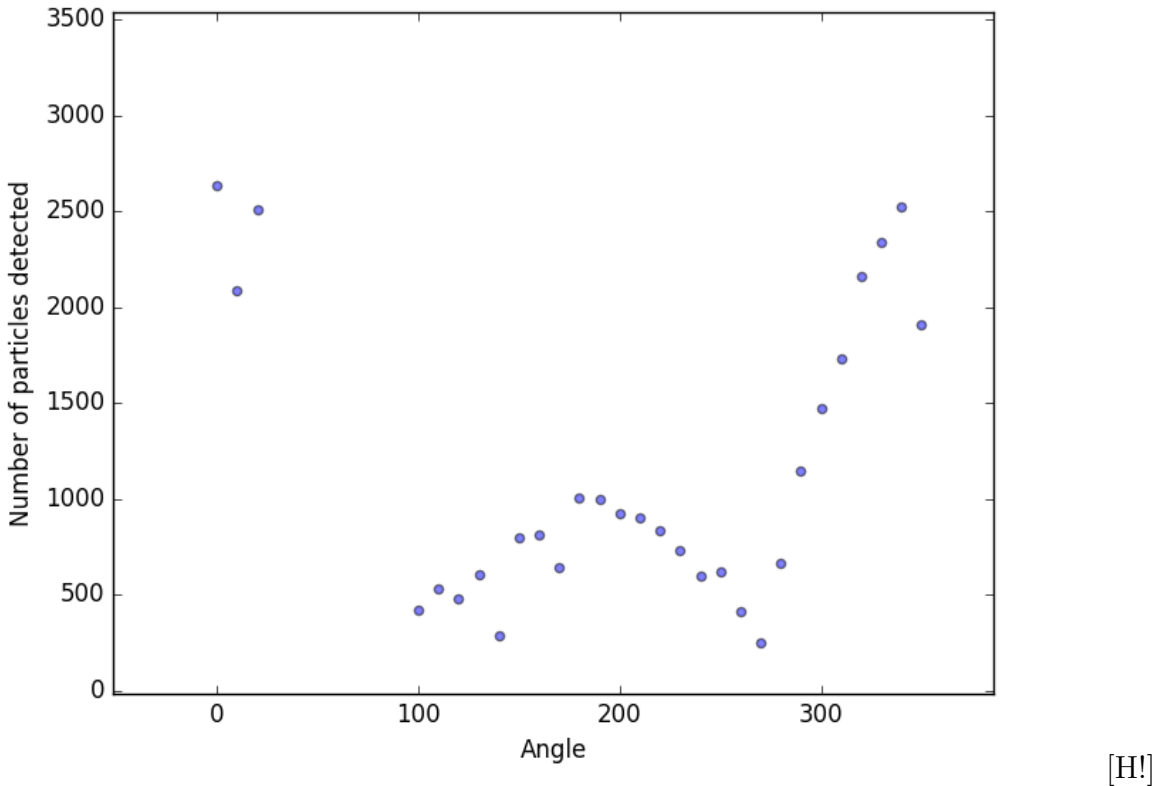


Figure 2.8: The amount of electrons detected from 100.000 shoot in the simulation [H!]

Secondly, the complex CAD model of the satellite –consisting of 7 modules, each with a give avarage material composition– was exported to Geant4. The scintillator and its read out was placed on the side of the satellite.

Thirdly, the γ absorption of the satellite was invastigated. Parallel γ -rays with a flux and energy distribution of GRB 9900123 (fig. 1.3) was simulated. 36 positions were investigated by varying the incident angle of the γ s around the major axis of the satellite.

The results show...

Fourthly, the effect of cosmic radiation was invastigated by utilizing the energy spectra of cosmic protons and electrons at the altitude of 500km. The satellite was radiated by these particles in Geant4 in the same positions that were used for the γ -rays of GRB 9900123. The induced signal of these particles was determined. This needs to be minimalized as it "competes" with the signal of gamma particles from GRBs.

Acknowledgment

Gabor Galgóczi would like to thank Balázs Újvári for the fruitful discussions they had on Geant4 simulations. Useful comments on detectors made Dezsö Varga's advices on detectors were highly appreciated. András Pál made vital comments on the description of the electronics. Last but not least the author would like to thank Norbert Werner for the continued contributions to this work.

References

- [1] Mészáros P., 2006, Reports on Progress in Physics, 69, 2259
- [2] Vedrenne G., & Atteia J.-L., 2009, Gamma-Ray Bursts: The brightest explosions in the Universe, Springer Praxis Books in Astronomy and Planetary Sciences, Published in association with Praxis Publishing, UK
- [3] Kouveliotou C., Wijers R. A. M. J., & Woosley S., 2012, Gamma-ray Bursts, Cambridge, UK: Cambridge University Press
- [4] Gehrels N., & Mészáros P. 2012, Science, 337, 932
- [5] Klebesadel R. W., Strong I. B., & Olson R. A. 1973, The Astrophysical Journal, 182, L85
- [6] Kouveliotou C., Meegan C. A., Fishman G. J., et al. 1993, The Astrophysical Journal Letters, 413, L101
- [7] Balázs L. G., Bagoly Z., Horváth I., et al. 2003, Astronomy and Astrophysics, 401, 129
- [8] Mészáros A., Bagoly Z., Balázs L. G., & Horváth I. 2006, Astronomy and Astrophysics, 455, 785
- [9] Berger E. 2014, Annual Review of Astronomy and Astrophysics, 52, 43
- [10] Rees M. J., & Meszaros P. 1994, The Astrophysical Journal, 430, L93
- [11] van Paradijs J., Groot P. J., Galama T., et al. 1997, Nature, 386, 686
- [12] Paczynski B. 1986, The Astrophysical Journal, 308, L43
- [13] Fruchter A. S., Levan A. J., Strolger L., et al. 2006, Nature, 441, 463
- [14] <https://arxiv.org/abs/1710.05834>
- [15] Abbott B. P., Abbott R., Abbott T. D., et al. 2017, Physical Review Letters, 119, 161101
- [16] Tanvir N. R., Levan A. J., Fruchter A. S., et al. 2013, Nature, 500, 547
- [17] Zhang, B. 2011, Comptes Rendus Physique, 12, 206
- [18] Toma, K., Yoon, S.-C., & Bromm, V. 2016, Space Science Reviews, 202, 159
- [19] Goldstein A., et al., 2017, The Astrophysical Journal Letters, 848, L14

- [20] Savchenko V., et al., 2017, *The Astrophysical Journal Letters*, 848, L15
- [21] Troja E., et al., 2017, *Nature*, 551, 71
- [22] Evans P. A., Cenko S. B., Kennea J. A., et al. 2017, *Science*, 358, 1565
- [23] Loeb A., 2016, *The Astrophysical Journal Letters*, 819, L21
- [24] KAGRA Collaboration, Akutsu T., Ando M., et al. 2017, arXiv:1710.04823
- [25] Cavallari E., & Frontera F. 2017, *Space Science Reviews*, 212, 429
- [26] Atwood, W. B., & GLAST Collaboration 1994, *Nuclear Instruments and Methods in Physics Research A*, 342, 302
- [27] Cavallari E., & Frontera F. 2017, *Space Science Reviews*, 212, 429
- [28] Barthelmy S. D., Barbier L. M., Cummings J. R., et al. 2005, *Space Science Reviews*, 120, 143
- [29] Winkler C., Courvoisier T. J.-L., Di Cocco G., et al. 2003, *Astronomy and Astrophysics*, 411, L1
- [30] Tavani M., Barbiellini G., Argan A., et al. 2009, *Astronomy and Astrophysics*, 502, 995
- [31] Yamaoka K., Yoshida A., Nonaka Y. 2011, 32nd International Cosmic Ray Conference, 9, 111
- [32] Serino M., Sakamoto T., Kawai N., et al. 2014, *Publications of the Astronomical Society of Japan*, 66, 87
- [33] Produit N., Barao F., Deluit S., et al. 2005, *Nuclear Instruments and Methods in Physics Research A*, 550, 616
- [34] Sadovnichii V. A., Panasyuk M. I., Amelyushkin A. M., et al. 2017, *Space Science Reviews*, 212, 1705
- [35] Li T., Xiong S., Zhang S., et al. 2018, *Science China Physics, Mechanics, and Astronomy*, 61, 31011
- [36] Navalgund K. H., Suryanarayana Sarma K., Gaurav P. K., Nagesh G., & Annadurai M. 2017, *Journal of Astrophysics and Astronomy*, 38, 34
- [37] Lin R. P., Dennis B. R., Hurford G. J., et al. 2002, *Solar Physics*, 210, 3
- [38] Hurley K., Mitrofanov I. G., Golovin D., et al. 2013, *EAS Publications Series*, 61, 459

- [39] Lipunov V., Kornilov V., Gorbovskoy E., et al. 2016, Revista Mexicana de Astronomia y Astrofisica Conference Series, 48, 42
- [40] Castro-Tirado A. J., Soldán J., Bernas M., et al. 1999, Astronomy and Astrophysics Supplement, 138, 583
- [41] Akerlof C. W., Kehoe R. L., McKay T. A., et al. 2003, Publications of the Astronomical Society of the Pacific, 115, 132
- [42] Majcher A., Batsch T., Castro-Tirado A. J., et al. 2015, Proceedings of SPIE, 9662, 966219
- [43] Gamma-Ray Bursts and Fast Transients Multi-wavelength Observations and Multi-messenger Signals,
R. Willingale, P. Mészáros
- [44] Nuclear Instruments and Methods in Physics Research A 506 (2003) 250-303
- [45] IEEE Transactions on Nuclear Science 53 No. 1 (2006) 270-278
- [46] Nuclear Instruments and Methods in Physics Research A 835 (2016) 186-225
- [47] Poole, C. M. and Cornelius, I. and Trapp, J. V. and Langton, C. M., A CAD Interface for GEANT4, Australasian Physical & Engineering Science in Medicine, 2012
- [48] <http://www.assimp.org/>
- [49] Hang Si. 2015. "TetGen, a Delaunay-Based Quality Tetrahedral Mesh Generator". ACM Trans. on Mathematical Software. 41 (2), Article 11 (February 2015), 36 pages
- [50] http://www.amcrys.com/pdf/4279_.pdf
- [51] http://www.hamamatsu.com/resources/pdf/ssd/s13360_series_kapd1052e.pdf
- [52] <http://multimedia.3m.com/mws/media/466120O/esr.pdf>
- [53] <https://arxiv.org/pdf/1311.7135.pdf>
- [54] <https://www.spenvis.oma.be/>

List of Figures

1.1	The life cycle of a massive star. When fusion stops the collapsing star releases energy in the form of jets observed as a gamma-ray burst	3
1.2	The light curves of 12 gamma-ray bursts observed by BATSE. The diversity of the curves is extraordinary. Events with a length from millisecond to a second exist either with smooth or highly variable curves.	4
1.3	The band function of GRB 990123 [43]	5
1.4	The field of view and localization accuracy of several missions including the Camelot CubeSat.	8
1.5	The modules of the satellite	10
1.6	Side extensions including of the CAMELOT satellite (left) where scintillators are placed and and a wrapped scintillator with the MPPC read out (right)	11
1.7	Energy spectra obtained by collecting the signal of 1 million γ with the one channel and the two channel read out	12
1.8	The Geant4 simulation of the whole ATLAS experiment	13
1.9	The scintillator on the left and the cage holding the setup on the right	13
1.10	The reflectivity [50] of the ESR tape that was used to wrap the scintillator in order to increase the light yield. This data was included in the simulation.	14
1.11	The emitted scintillation light spectra of three types of scintillators. In our experiment CsI(Tl) was used	15
1.12	The photon detection efficiency [51] of the MPPCs used for the readout of the scintillators. This data was included in the simulation.	16
1.13	The schematic design of the readout of the MPPC for the 1 channel configuration	17
1.14	The schematic design of the readout electronics of the 2 channel setup	17
1.15	The ^{241}Am <i>gamma</i> source was placed in a collimator system as can be seen on the image	18
1.16	The MPPCs for the 2 channel readout are positioned symmetrically from the center of the scintillator	19
1.17	Simulation of 100 γ s emitted from the source. The blue lines represent the track of the γ s and the green lines represent the track of the optical photons created by scintillation. Only the photons that were detected are drawn.	19

1.18	The CAD model of the satellite (on the right) and the view of the imported model in Geant (on the left)	20
1.19	The satellite radiated by a pencil beam of 10.000 γ particles. The scattered γ s induce signal in the scintillator	21
2.1	The obtained energy spectra from simulation with and without x-ray fluorescence being turned on. One can see that, the first peak, which can be seen in the experiments only appear when x-ray fluorescence was turned on.	22
2.2	The positions of irradiation for the investigation of the response of the scintillator	23
2.3	The spectra of 11 million photons taken experimentally (blue histogram) matched up with the results of the simulation (green histogram) and the Gaussian fitted to the simulated data	25
2.4	The spatially avaraged band function (differential flux for a given energy band, solid line) and the integrated band function (dotted line) of electrons at an altitude of 500 km for solar minimum (left) and solar maximum (right)	27
2.5	The spatially avaraged band function (differential flux for a given energy band, solid line) and the integrated band function (dotted line) of protons at an altitude of 500 km for solar minimum (left) and solar maximum (right)	27
2.6	The spectrum measured when the electrons were shot perpendicular to the scintillator (called angle of 0 °)	28
2.7	The CAD model of the satellite (on the right) and the view of the imported model in Geant (on the left)	28
2.8	The ammount of electrons detected from 100.000 shoot in the simulation	29

NYILATKOZAT

Név:

ELTE Természettudományi Kar, szak:

NEPTUN azonosító:

Diplomamunka címe:

A **diplomamunka** szerzőjeként fegyelmi felelősségem tudatában kijelentem, hogy a dolgozatom önálló munkám eredménye, saját szellemi termékem, abban a hivatkozások és idézések standard szabályait következetesen alkalmaztam, mások által írt részeket a megfelelő idézés nélkül nem használtam fel.

Budapest, 20

a hallgató aláírása